Supporting Information: Solvent effects on the second harmonic responses of donor–acceptor Stenhouse adducts: from implicit to hybrid solvation models

Angela Dellai,[†] Isabella Krismer,[†] Giacomo Prampolini,[‡] Benoît Champagne,[¶] Tárcius N. Ramos,[*,¶] and Frédéric Castet[*,†]

[†]*Univ. Bordeaux, CNRS, Bordeaux INP, Institut des Sciences Moléculaires, UMR 5255, F-33400 Talence, France*

[‡]*Consiglio Nazionale delle Ricerche, CNR-ICCOM, Pisa, Italy*

[¶]*Unité de Chimie Physique Théorique et Structurale, Chemistry Department, Namur Institute of Structured Matter, University of Namur, Belgium*

E-mail: tarcius.nascimento@unamur.be; frederic.castet@u-bordeaux.fr

Contents

1 Additional details on experimental and computational methodologies

1.1 Experimental determination of β_{HRS} and DR

The experimental NLO responses of the BA4 chromophore have been reported in Ref. S1, while the experimental setup was extensively described in Refs. S1–S3. HRS measurements were carried out at room temperature using the chloroform solvent as internal reference.[S4] The incident excitation wavelength of 1300 nm was chosen to avoid both absorption of the fundamental beam from chloroform in the near IR range (ω) and absorption of the scattered harmonic beam (2ω) from the sample.

For a diluted binary solution composed of a solvent (S = chloroform) and a solute (X = BA4), the total incoherent scattered second-harmonic (HRS) light is given by:

$$I_{2\omega}^{\Psi V} = A(F^L)^2\{\left[|\beta_S|^2 C_S^{\Psi V}\right] N_S + \left[|\beta_X|^2 C_X^{\Psi V}\right] N_X\} I_\omega^2 10^{-\epsilon_{2\omega}\delta C_X} \tag{S1}$$

where the orientational average for the solvent ($i = S$) and the solute ($i = X$) are defined as:

$$C_i^{\Psi V} = \cos^4\Psi + (1 + DR_i)\cos^2\Psi\sin^2\Psi + DR_i\sin^4\Psi \tag{S2}$$

As described below, the experimental protocol involved two independent sets of measurements to access the β_{HRS} and DR values of the solute from equations S1 and S2.

1.1.1 Quadratic dependence of the HRS Signal through power scans

The HRS amplitudes were first obtained by performing power scans, *i.e.* by determining the coefficient of the quadratic dependence of the scattered intensity (equation S1) as a function of the incident intensity and for different solute concentrations. The polarization configuration was set to vertical-vertical (VV), *i.e.* with vertically polarized incident light

($\Psi = 90°$) and scattered light also analyzed vertically. Power scans were performed on diluted solutions at different concentrations (varying from 10^{-4} to 10^{-6} mol/L). The coefficient of quadratic dependence was obtained by fitting the power curves (see Figures S1) as a function of the incident power (I_ω) and solute concentration (N_X) using a 2D fitting function of the form:

$$I_{2\omega}^{VV} = (p_1 + p_2 N_X)(I_\omega - p_3)^2 \tag{S3}$$

where p_i ($i = 1$–3) are (all positive) fitting parameters. The extracted quantity is:

$$C_X^{VV}|\beta_X|^2 \equiv \langle \beta_{ZZZ}^2 \rangle = R.p_2/p_1 \tag{S4}$$

where $R = N_S C_S^{VV}|\beta_S|^2$ is the chloroform contribution. In Ref. S1, chloroform was used as internal reference and its contribution assumed equal to $R = 6088$ a.u. Note that both the instrumental factor A and the local field correction F^L cancel out in equation S4 through the p_2/p_1 ratio, allowing simple and direct determination of the solute contribution from a concentration series. However, it is important to mention that the reference value of 6088 a.u. used for the chloroform contribution is itself calibrated (following the procedure detailed by Kaatz and Shelton in Ref. S5) with respect to an absolute reference, namely the liquid carbon tetrachloride (CCl_4), for which the only non zero molecular (incoherent) component of the first hyperpolarizability tensor, β_{xyz}, is equal to 38 a.u.[S4] Since $CHCl_3$ and CCl_4 have different refractive indices at optical frequencies, the calibration process involves a correction term corresponding to the ratio between the corresponding Lorentz local field factors. However, the F^L values of the two solvents are very similar, ($F_{CHCl_3}^L = 2.5$ and $F_{CCl_4}^L = 2.57$), so that introducing such a correction has no significant effect.

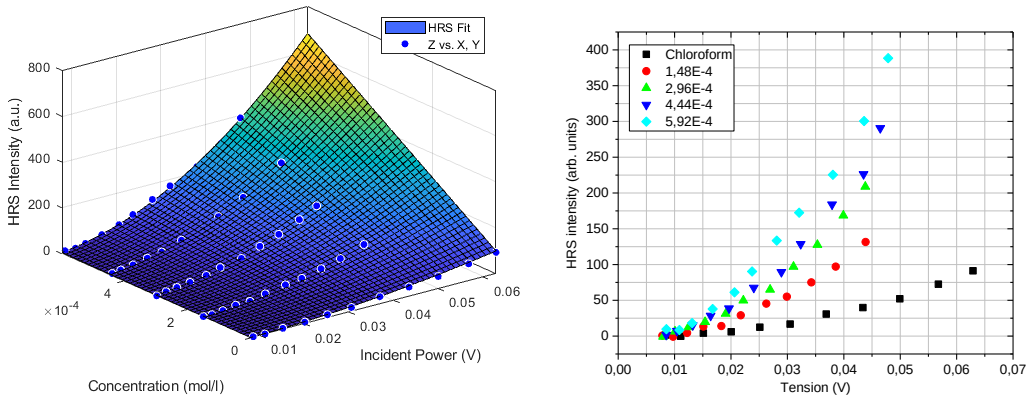

Figure S1: Intensity of the harmonic scattered light as a function of the chromophore concentration and incident power (taken from Ref. S1).

1.1.2 Determination of the depolarization ratio and total HRS response through polarization scans

The depolarization ratio of the chromophore (DR) was obtained by performing polarization scans, *i.e.* through stepwise variation of the polarization plane of the incident light, at constant incident power. To extract the chromophore contribution, the scattered intensity of the binary solution was measured for the pure solvent, as well as for the most concentrated binary solution. The polarization configuration was set to Ψ-V (where Ψ is the variable angle of the half-wave plate) for the incident and scattered lights, respectively. The DR values were determined by fitting the polarization curves (see Figures S2) using a constrained fitting function of the form:

$$I_{2\omega}^{\Psi V} = B\left(\cos^4(\Psi-\Psi_0) + (1+DR_i)\cos^2(\Psi-\Psi_0)\sin^2(\Psi-\Psi_0) + DR_i\sin^4(\Psi-\Psi_0)\right) \quad \text{(S5)}$$

where the intensity factor B, the angular offset Ψ_0 and the depolarization ratio DR_i are fitting parameters.

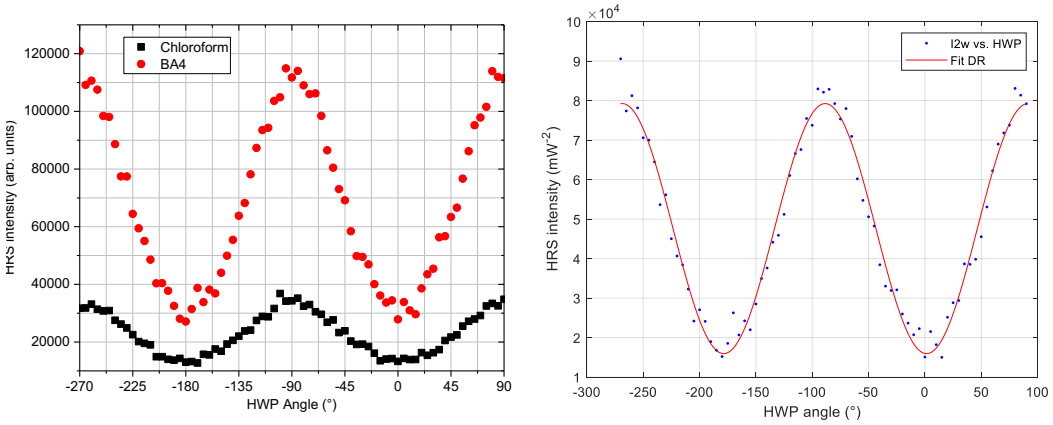

Figure S2: Left: Intensity of the harmonic scattered light as a function of the (linear) polarization angle of the incident light for the solvent (black) and the binary solution (red). Right: Intensity difference (points) and fitted curve. Taken from Ref. S1.

The NLO quantities determined for BA4 using the 2-step experimental protocol described above, as well as their uncertainty, are reported in Table S1.

Table S1: NLO quantities and their uncertainty for BA4: coefficient of quadratic dependence of the scattered intensity as a function of incident intensity obtained by performing a power scan ($C_X^{VV}|\beta_X|^2$, a.u.), depolarization ratio obtained by performing a polarization scan (DR), and total hyperpolarizability (β_{HRS}, a.u.). Last two columns report the coefficient of determination (R^2) for the power scan (2D fit) and polarization scan (Ψ fit). Taken from Ref. S1.

	$C_X^{VV}\|\beta_X\|^2$	DR	β_{HRS}	R^2 [2D fit]	R^2 [Ψ fit]
Value	6.15×10^7	5.0	8600	0.99	0.98
Uncertainty	2.32×10^6	0.3	390	-	-

1.2 Relations between the $\langle\beta^2_{ZZZ}\rangle$ and $\langle\beta^2_{ZXX}\rangle$ orientational invariants and the molecular β-tensor components

$$\begin{aligned}
\langle\beta^2_{ZZZ}\rangle = &\frac{1}{7}\sum_{\zeta}^{x,y,z}\beta^2_{\zeta\zeta\zeta} + \frac{4}{35}\sum_{\zeta\neq\eta}^{x,y,z}\beta^2_{\zeta\zeta\eta} + \frac{2}{35}\sum_{\zeta\neq\eta}^{x,y,z}\beta_{\zeta\zeta\zeta}\beta_{\zeta\eta\eta} \\
&+ \frac{4}{35}\sum_{\zeta\neq\eta}^{x,y,z}\beta_{\eta\zeta\zeta}\beta_{\zeta\zeta\eta} + \frac{4}{35}\sum_{\zeta\neq\eta}^{x,y,z}\beta_{\zeta\zeta\zeta}\beta_{\eta\eta\zeta} + \frac{1}{35}\sum_{\zeta\neq\eta}^{x,y,z}\beta^2_{\eta\zeta\zeta} \\
&+ \frac{4}{105}\sum_{\zeta\neq\eta\neq\xi}^{x,y,z}\beta_{\zeta\zeta\eta}\beta_{\eta\xi\xi} + \frac{1}{105}\sum_{\zeta\neq\eta\neq\xi}^{x,y,z}\beta_{\eta\zeta\zeta}\beta_{\eta\xi\xi} \\
&+ \frac{4}{105}\sum_{\zeta\neq\eta\neq\xi}^{x,y,z}\beta_{\zeta\zeta\eta}\beta_{\xi\xi\eta} \\
&+ \frac{2}{105}\sum_{\zeta\neq\eta\neq\xi}^{x,y,z}\beta^2_{\zeta\eta\xi} + \frac{4}{105}\sum_{\zeta\neq\eta\neq\xi}^{x,y,z}\beta_{\zeta\eta\xi}\beta_{\eta\zeta\xi}
\end{aligned} \tag{S6}$$

$$\begin{aligned}
\langle\beta^2_{ZXX}\rangle = &\frac{1}{35}\sum_{\zeta}^{x,y,z}\beta^2_{\zeta\zeta\zeta} + \frac{4}{105}\sum_{\zeta\neq\eta}^{x,y,z}\beta_{\zeta\zeta\zeta}\beta_{\zeta\eta\eta} - \frac{2}{35}\sum_{\zeta\neq\eta}^{x,y,z}\beta_{\zeta\zeta\zeta}\beta_{\eta\eta\zeta} \\
&+ \frac{8}{105}\sum_{\zeta\neq\eta}^{x,y,z}\beta^2_{\zeta\zeta\eta} + \frac{3}{35}\sum_{\zeta\neq\eta}^{x,y,z}\beta^2_{\zeta\eta\eta} - \frac{2}{35}\sum_{\zeta\neq\eta}^{x,y,z}\beta_{\zeta\zeta\eta}\beta_{\eta\zeta\zeta} \\
&+ \frac{1}{35}\sum_{\zeta\neq\eta\neq\xi}^{x,y,z}\beta_{\zeta\eta\eta}\beta_{\zeta\xi\xi} - \frac{2}{105}\sum_{\zeta\neq\eta\neq\xi}^{x,y,z}\beta_{\zeta\zeta\xi}\beta_{\eta\eta\xi} \\
&- \frac{2}{105}\sum_{\zeta\neq\eta\neq\xi}^{x,y,z}\beta_{\zeta\zeta\eta}\beta_{\eta\xi\xi} \\
&+ \frac{2}{35}\sum_{\zeta\neq\eta\neq\xi}^{x,y,z}\beta^2_{\zeta\eta\xi} - \frac{2}{105}\sum_{\zeta\neq\eta\neq\xi}^{x,y,z}\beta_{\zeta\eta\xi}\beta_{\eta\zeta\xi}
\end{aligned} \tag{S7}$$

1.3 Solvent Embedding Potential used in QM/MM calculations

Table S2: Point charges and polarizabilities used in QM/MM calculations (all values are in a.u.).

Atom	q	α
Cl	0.02469	14.29891
C	0.34805	12.68519
H	0.27398	2.61349

1.4 Benchmark calculations to define the QM' level of approximation in ONIOM

In Tables S3 and S4, we report the static ($\omega \to 0$) and frequency-dependent ($\omega = 1300$ nm) HRS responses of the open and closed forms of BA4, calculated for a small set of snapshots using the hybrid QM/QM' (ONIOM) approach with various QM' levels. For each snapshot, the line labelled "none" corresponds to the NLO responses calculated at the SMD:M06-2X/6-311+G(d) level, with no explicit solvent molecule, while 6-311+G(d) refers to the reference values (*i.e.* the NLO responses of the full system including both the BA4 chromophore and explicit chloroform molecules were calculated at the SMD:M06-2X/6-311+G(d) level), from which the relative errors of the ONIOM calculations were computed. Figure S3 displays a graphic representation of the relative errors listed in Tables S3 and S4, where squared and cross marks correspond to the MSE of frequency-dependent and static β_{HRS}^{ONIOM} values, respectively.

Table S3: Static (β^0_{HRS}) and frequency-dependent (β^ω_{HRS}) HRS hyperpolarizability (in a.u.) of the **open form** calculated using ONIOM(`High:Low`), with `High` = M06-2X/6-311+G(d) and with various `Low` levels. The total CPU time (in hours) for the calculation of the full system (chromophore + solvent molecules) with the Low level is reported. For assessing the relative error values, quantified by the mean signed error (MSE %), the M06-2X/6-311+G(d) level was taken as the reference value.

	Snapshot	50	100	150	200	341	571	665	790	901
none	CPU Time	13	14	13	13	14	17	14	13	13
	β^ω_{HRS}	9509	18133	4817	12387	8333	10498	6564	9405	16054
	β^0_{HRS}	5133	7983	3284	5900	5200	5031	3810	4239	7308
6-311+G(d)	CPU Time	142	184	95	133	132	168	103	100	125
	β^ω_{HRS}	4841	11081	7475	7354	7575	11588	4586	6292	11731
	β^0_{HRS}	2908	5506	5134	3854	4905	4962	3179	3495	5356
6-311G(d)	CPU Time	24	28	20	23	24	26	24	20	28
	β^ω_{HRS}	5318	12204	6911	7888	8087	12377	4760	6540	11812
	MSE (%)	*10*	*10*	*-8*	*7*	*7*	*7*	*4*	*4*	*1*
	β^0_{HRS}	3167	6089	4459	3889	5320	5336	3302	3603	5358
	MSE (%)	*9*	*11*	*-13*	*1*	*8*	*8*	*4*	*3*	*0*
6-31+G(d)	CPU Time	98	95	64	64	85	80	66	53	79
	β^ω_{HRS}	4744	11451	7012	6879	7980	11997	4567	6347	11665
	MSE (%)	*-2*	*3*	*-6*	*-6*	*5*	*4*	*0*	*1*	*-1*
	β^0_{HRS}	2928	5622	4282	3574	5102	4925	3199	3530	5337
	MSE (%)	*1*	*2*	*-17*	*-7*	*4*	*-1*	*1*	*1*	*0*
6-31G(d)	CPU Time	16	22	18	16	16	17	14	15	16
	β^ω_{HRS}	5132	12275	7103	7658	8720	11830	4701	6570	11847
	MSE (%)	*6*	*11*	*-5*	*4*	*15*	*2*	*2*	*4*	*1*
	β^0_{HRS}	3098	6219	4628	3840	5647	5366	3321	3700	5369
	MSE (%)	*7*	*13*	*-10*	*0*	*15*	*8*	*4*	*6*	*0*
6-31G	CPU Time	12	17	11	12	12	13	14	14	12
	β^ω_{HRS}	4127	12430	8634	6520	9495	13416	4615	6599	10373
	MSE (%)	*-15*	*12*	*16*	*-11*	*25*	*16*	*1*	*5*	*-12*
	β^0_{HRS}	2782	6296	5397	3487	6096	5917	3417	3869	4721
	MSE (%)	*-4*	*14*	*5*	*-10*	*24*	*19*	*7*	*11*	*-12*
4-31G	CPU Time	12	13	11	14	11	15	11	11	14
	β^ω_{HRS}	4190	12139	8133	6742	9749	12700	4504	6533	10663
	MSE (%)	*-13*	*10*	*9*	*-8*	*29*	*10*	*-2*	*4*	*-9*
	β^0_{HRS}	2794	6260	5219	3535	6257	5819	3336	3848	4831
	MSE (%)	*-4*	*14*	*2*	*-8*	*28*	*17*	*5*	*10*	*-10*

Table S4: Static (β^0_{HRS}) and frequency-dependent (β^ω_{HRS}) HRS hyperpolarizability (in a.u.) of the **closed form** calculated using ONIOM(`High:Low`), with `High` = M06-2X/6-311+G(d) and with various `Low` levels. The total CPU time (in hours) for the calculation of the full system (chromophore + solvent molecules) with the Low level is reported. For assessing the relative error values, quantified by the mean signed error (MSE %), the M06-2X/6-311+G(d) level was taken as the reference value.

	Snapshot	50	100	150	200	341	571	665	790	901
none	CPU Time	11	23	13	20	20	20	19	19	19
	β^ω_{HRS}	354	324	306	295	285	318	373	360	322
	β^0_{HRS}	397	363	347	326	313	341	396	383	351
6-311+G(d)	CPU Time	111	117	156	175	102	133	123	125	145
	β^ω_{HRS}	308	304	960	227	304	864	2373	568	544
	β^0_{HRS}	353	365	1006	271	342	936	2473	593	600
6-311G(d)	CPU Time	29	28	29	31	24	27	28	27	27
	β^ω_{HRS}	332	270	220	232	266	301	355	322	313
	MSE (%)	*8*	*-11*	*-77*	*2*	*-13*	*-65*	*-85*	*-43*	*-43*
	β^0_{HRS}	377	318	258	269	301	339	407	359	364
	MSE (%)	*7*	*-13*	*-74*	*-1*	*-12*	*-64*	*-84*	*-40*	*-39*
6-31+G(d)	CPU Time	80	62	78	101	57	80	80	69	79
	β^ω_{HRS}	295	274	318	239	248	261	334	341	300
	MSE (%) *-4*	*-10*	*-67*	*5*	*-19*	*-70*	*-86*	*-40*	*-45*	
	β^0_{HRS}	344	325	381	286	287	305	390	387	361
	MSE (%)	*-3*	*-11*	*-62*	*5*	*-16*	*-67*	*-84*	*-35*	*-40*
6-31G(d)	CPU Time	20	19	27	26	20	19	18	21	27
	β^ω_{HRS}	316	271	224	248	249	283	326	291	302
	MSE (%)	*3*	*-11*	*-77*	*9*	*-18*	*-67*	*-86*	*-49*	*-45*
	β^0_{HRS}	362	317	264	286	284	319	372	326	350
	MSE (%)	*2*	*-13*	*-74*	*6*	*-17*	*-66*	*-85*	*-45*	*-42*
6-31G	CPU Time	22	23	21	15	14	16	20	16	21
	β^ω_{HRS}	309	266	226	246	252	286	342	288	307
	MSE (%)	*0*	*-12*	*-77*	*8*	*-17*	*-67*	*-86*	*-49*	*-44*
	β^0_{HRS}	355	313	266	284	287	322	388	324	357
	MSE (%)	*1*	*-14*	*-74*	*5*	*-16*	*-66*	*-84*	*-45*	*-41*
4-31G	CPU Time	16	16	20	15	19	20	15	15	15
	β^ω_{HRS}	328	277	245	270	240	292	324	299	301
	MSE (%)	*6*	*-9*	*-74*	*19*	*-21*	*-66*	*-86*	*-47*	*-45*
	β^0_{HRS}	374	332	284	311	274	326	367	332	348
	MSE (%)	*6*	*-9*	*-72*	*15*	*-20*	*-65*	*-85*	*-44*	*-42*

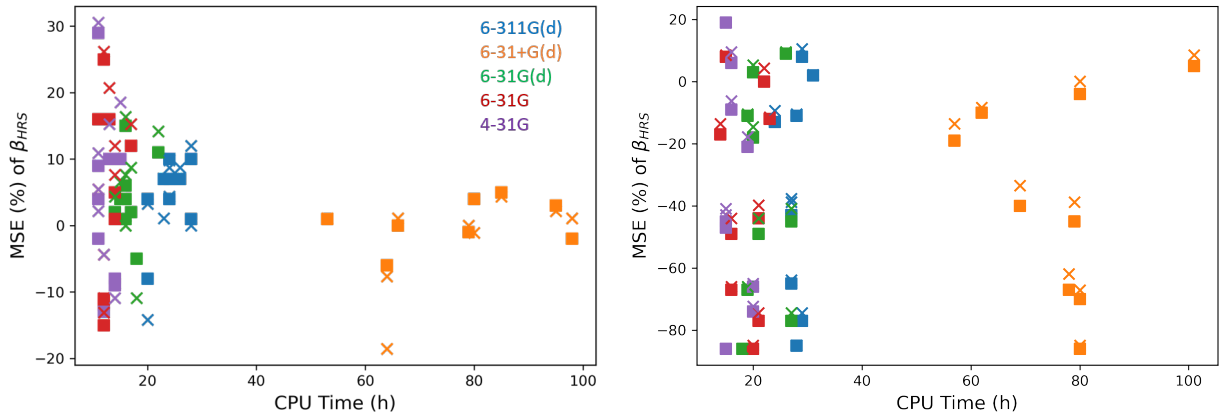

(a) Open (b) Closed

Figure S3: Mean signed errors (MSE %) on the frequency-dependent (squared marks) and static (cross marks) β_{HRS}^{ONIOM} values calculated for a) open and b) closed isomers using different `Low` levels, with respect to reference M06-2X/6-311+G(d) calculations.

As illustrated in Figure S3, the CPU time rises considerably with the extent of the Gaussian basis set used in the QM' level. While an ONIOM calculation using the 4-31G basis set for the `Low` level takes between 11 and 20 hours to reach termination, the reference calculation using the 6-311+G(d) basis set needs between 3 to 8 days to complete. Errors calculated for the closed form are more pronounced than for the open form, for which the 4-31G basis set provides errors already below 30%. From these analyses, the basis set selected for the `Low` layer is 6-31G(d) due to its acceptable compromise between time (around 1 day of CPU time) and accuracy (the MSE is reduced to 15% in the case of the open form).

2 Additional results

2.1 Polarizable continuum models

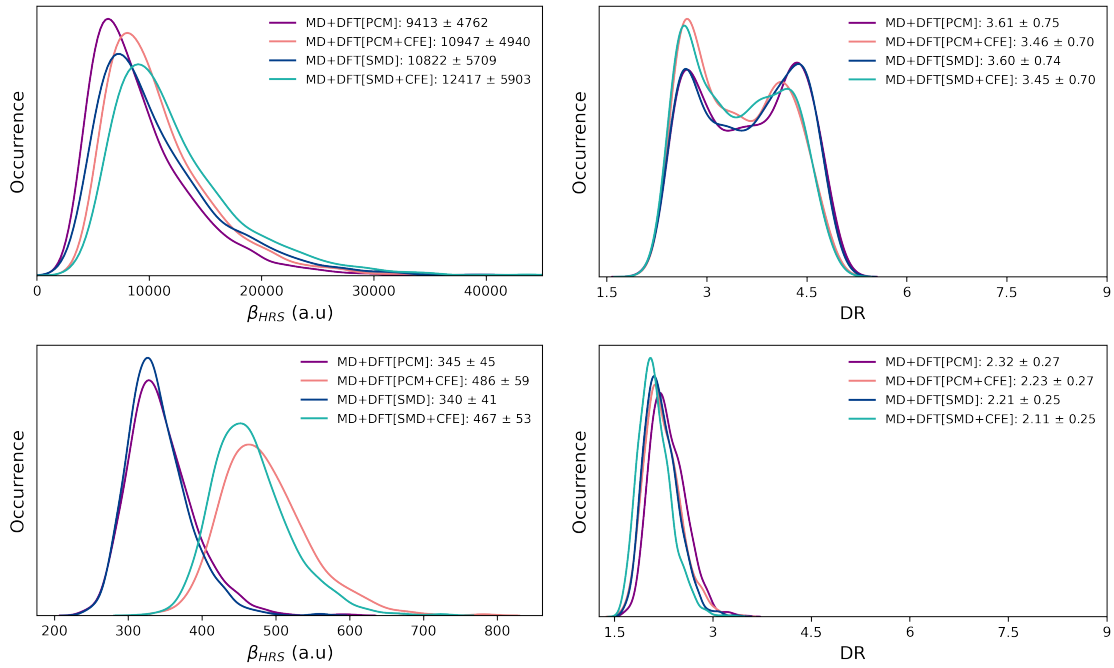

Figure S4: Statistical distributions (kernel density estimations) of the frequency-dependent (λ = 1300 nm) HRS first hyperpolarizability (left) and depolarization ratio (right) of the open (top) and closed (bottom) forms, as calculated using the MD+DFT[SOLV] scheme at the CAM-B3LYP/6-311+G(d) level with various solvation schemes. Average and standard deviation values are reported in the legends.

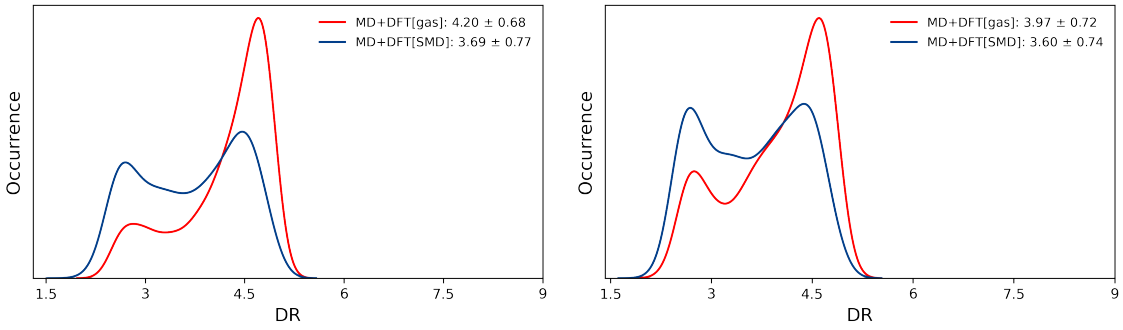

Figure S5: Statistical distributions (kernel density estimations) of the depolarization ratio of the open form, as calculated using the MD+DFT[gas] and MD+DFT[SMD] schemes at the M06-2X/6-311+G(d) (left) and CAM-B3LYP/6-311+G(d) (right) levels. Average and standard deviation values are reported in the legends.

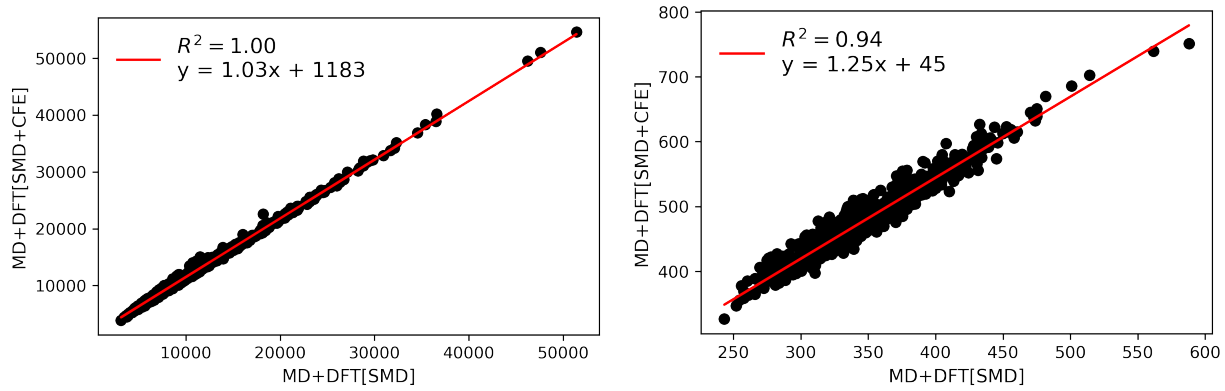

(a) Open (b) Closed

Figure S6: Linear correlation between HRS first hyperpolarizabilities computed using the MD+DFT[SMD] and MD+DFT[SMD+CFE] schemes (at the M06-2X level) for the open (a) and closed (b) isomers.

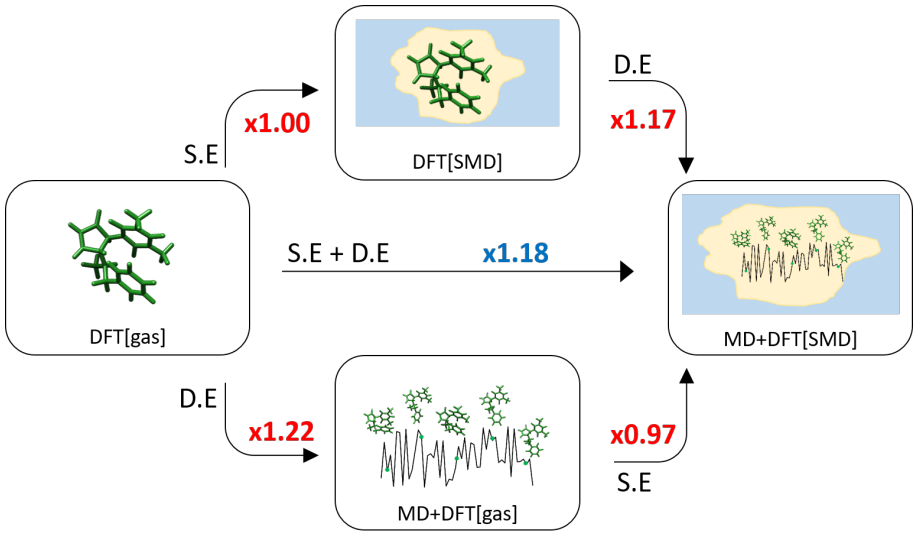

Figure S7: Enhancement factors (in red) of the HRS first hyperpolarizability of the closed form computed at the M06-2X level due to the inclusion of structural dynamic and solvent effects (labeled as D.E and S.E, respectively). In blue is reported the value of the enhancement factor from DFT[gas] to MD+DFT[SMD] where both structural dynamic and solvent effects are simultaneously included.

2.2 QM/MM calculations

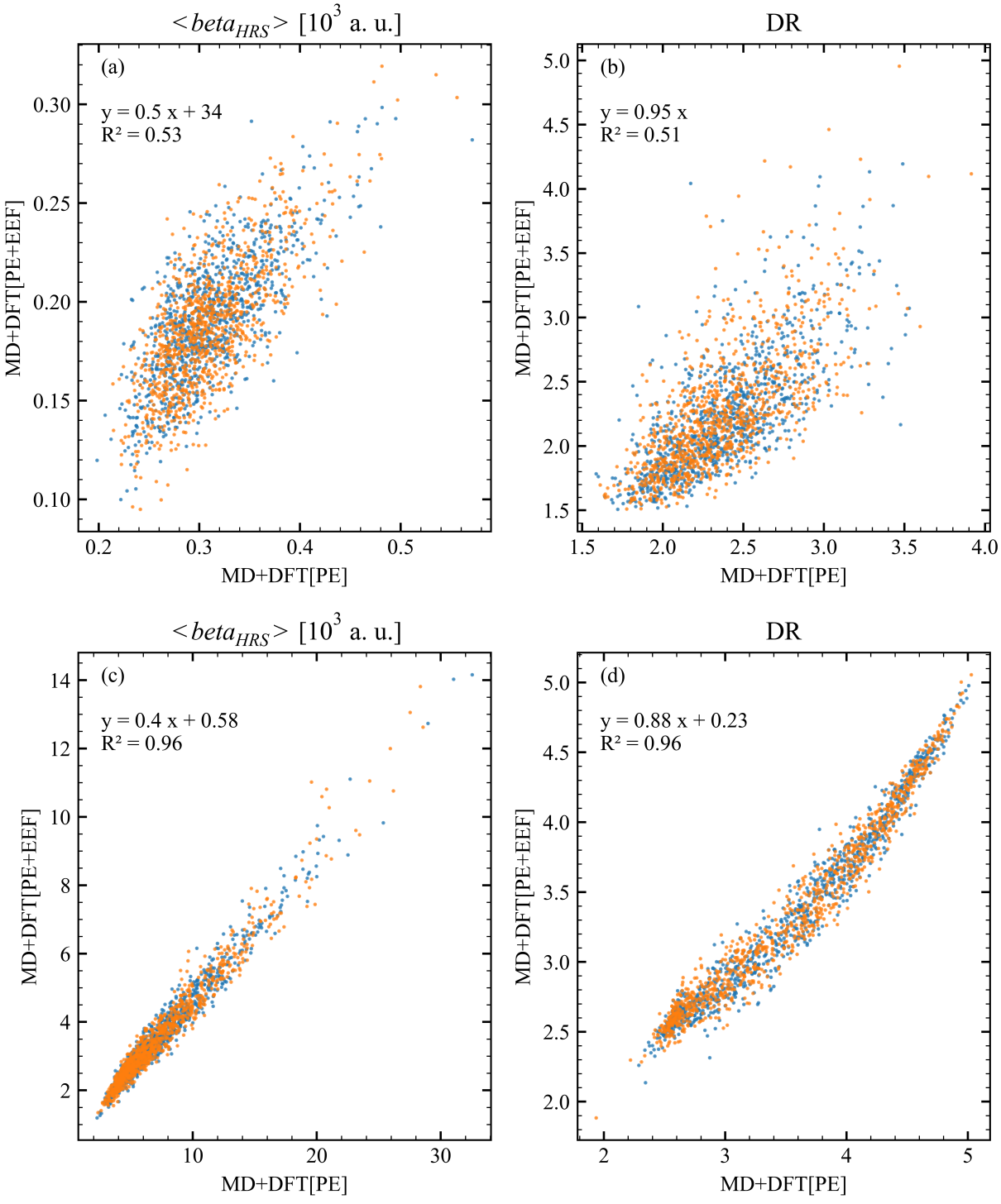

Figure S8: Linear correlation between HRS the first hyperpolarizability and DR computed using the MD+DFT[PE] and MD+DFT[PE+EEF] schemes (at the CAM-B3LYP level), for the closed (a and b) and open (c and d) forms.

2.2.1 Statistical convergence of the sampling

Two independent MD simulations provided each a set containing 1000 snapshots equally spaced in time to evaluate the statistical convergence of the NLO properties, as calculated using the MD+DFT[PE] model. Similar distributions of values were obtained between both sets, as presented in Figures S9. As discussed in the main text, the asymmetric shape of β_{HRS} of the open form is related to an enhancement due to structural changes from the equilibrium (minimum energy) geometry. Although the DR mean and median values are similar, a bimodal distribution is observed for the open form (with one narrow distribution centered around 2.7 and one broader around 4.3). Although this bimodal profile suggests in first analysis the existence of two qualitatively different harmonophores, Figure S5 shows that it also originates from solvent effects, since the peak at $DR = 2.7$ is much smaller when calculations are carried out in the gas phase. This strong contribution of solvent effects in the relative intensity of the two peaks is consistent with the fact that no correlation could be drawn between structural and NLO properties (see Section 2.2.3). This is also consistent with the evolution of DR values plotted against β_{HRS} values, which shows a denser distribution close to the equilibrium geometry ($DR = 2.5$) than away from equilibrium with DR reaching 5.0 (see Figure S16) when solvent effects are included, for instance using MD+DFT[PE].

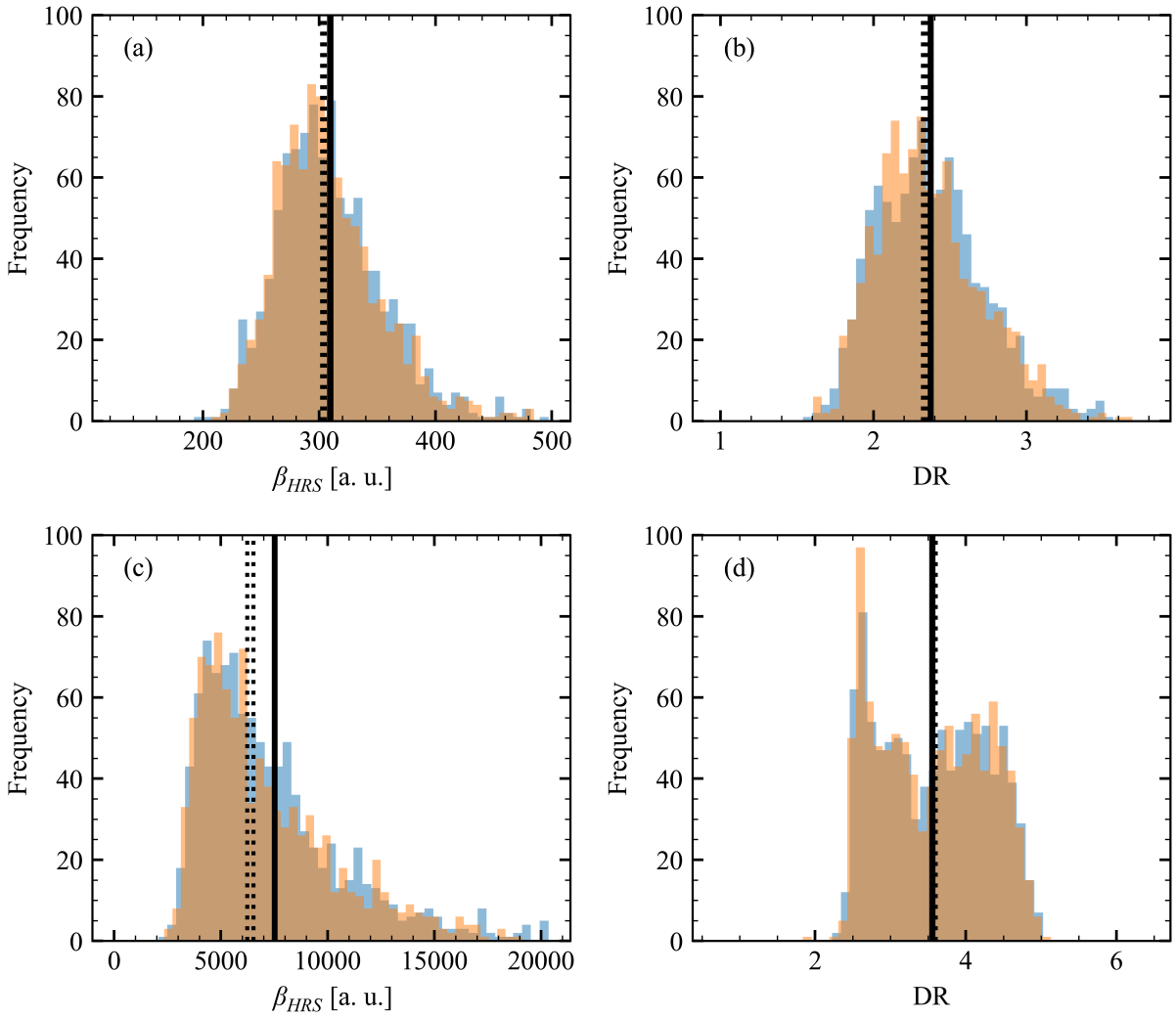

Figure S9: Distributions of the optical properties calculated on two independent sets of samplings (blue and orange) with their respective mean (full line) and median (dashed line). The calculations were performed on the MD+DFT[PE] model at the MD+DFT[PE]/CAM-B3LYP/6-311+G(d) level for the closed (a and b) and open (c and d) forms for frequency-dependent responses ($\lambda = 1300$ nm).

The quality of the mean values was assessed by computing the mean as a function of the sampling size. The V_{ref} reference values are those obtained over the 2000 configurations, encompassing the two sets, and the relative errors [$RE = (V - V_{ref})/V_{ref}$] were evaluated by splitting each set in $N = 100$, 125, 200, 250, 500, and 1000 configurations equally spaced in time, ensuring that the snapshots cover the whole trajectory for every N. Figures S10 show the RE evolution of the β_{HRS} and DR properties. Generally, the RE values oscillate until

$N = 250$ and then converge smoothly up to $N = 1000$. Although errors smaller than 2% and 10% were obtained using only 100 configurations for the closed and open forms, respectively, all the results reported are average over 1000 configurations.

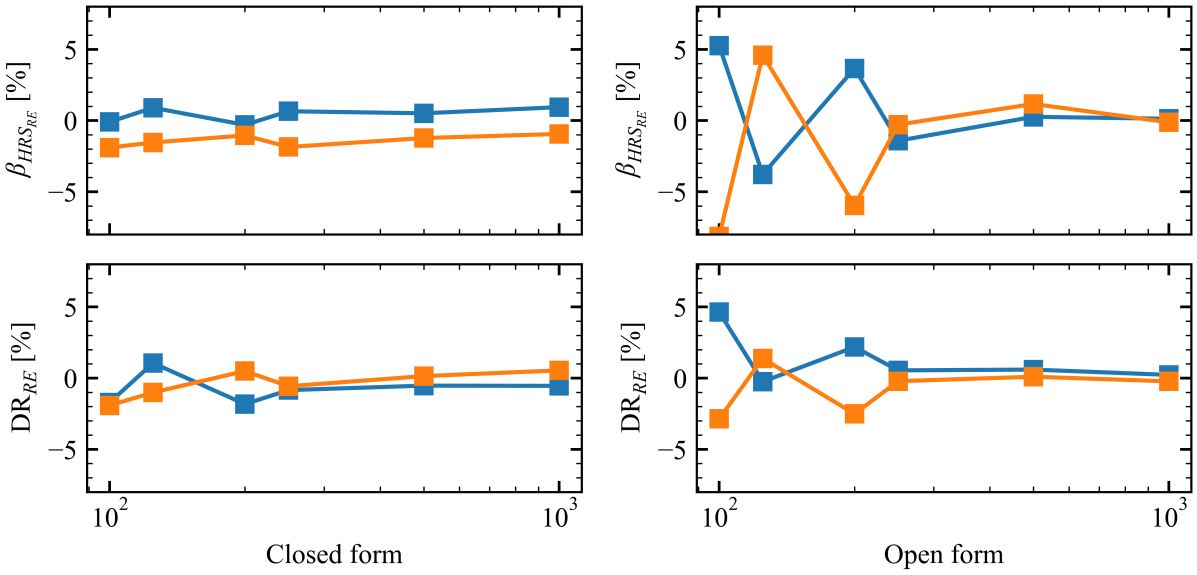

Figure S10: Relative error on calculating the mean values of β_{HRS} and DR considering an increasing size of the equally space sampling points for two independent sets. $X_{RE} = (X - X_{ref})/X_{ref}$ where $X = \beta_{HRS}$ or DR, and the reference values are the averages over 2000 configurations. The calculations were performed at the MD+DFT[PE]/CAM-B3LYP/6-311+G(d) level for frequency-dependent responses ($\lambda = 1300$ nm).

2.2.2 Structural analyses

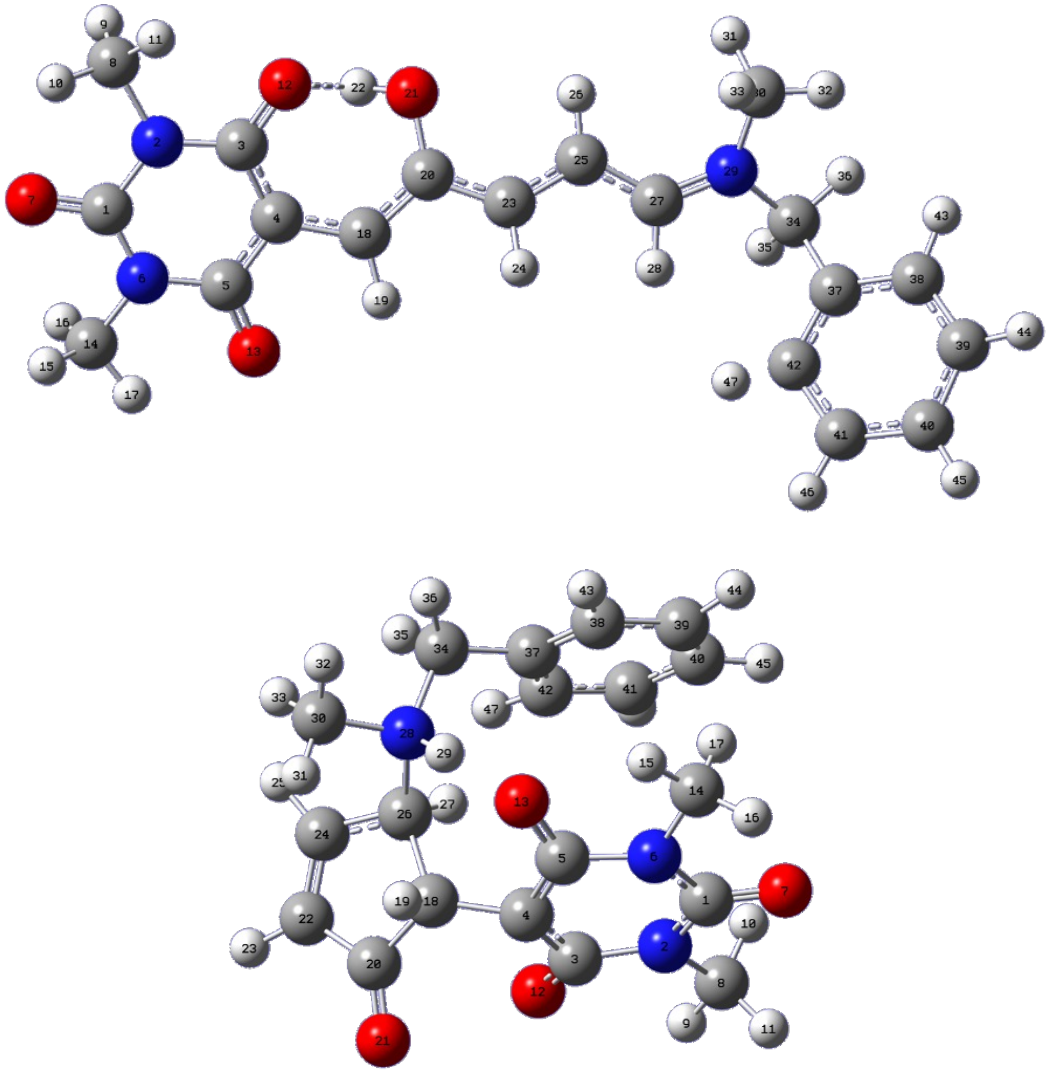

Figure S11: Structure and atom labeling of the open (top) and closed (bottom) conformers.

The distribution of the bond values and dihedral angles of the conjugated chain were evaluated in order to obtain the bond length alternation (BLA) of the open and closed isomers, and the parameter P as defined below:

$$BLA(open) = \frac{b_{4,18} + b_{20,23} + b_{25,27} + b_{29,34}}{4} - \frac{b_{18,20} + b_{23,25} + b_{27,29} + b_{34,37}}{4} \qquad \text{(S8)}$$

$$BLA(closed) = \frac{b_{4,18} + b_{26,28} + b_{34,37}}{3} - \frac{b_{18,26} + b_{28,34}}{2} \tag{S9}$$

$$P = \ln\left(\prod_i |\cos\theta_i|\right) \tag{S10}$$

$b_{i,j}$ is the bond length between atoms i and j, and θ_i is the dihedral angle around the $b_{i,j}$ bond. P sums to zero for a perfect planar conjugation path ($\cos\theta_i = 1$) and tends to $-\infty$ if at least one dihedral angle is equal to 90°. Other interesting structural parameters are the distance between atoms 1 and 40, which provides information about how linear or bent the molecule is, and the distance between atoms 12 and 22 for the open form. The results in Figures S12 and S13 show that the closed form presents bent configurations and more negative P values. By assuming that all the angles are the same, the mean $P = -6.03$ value leads to $\theta_i \simeq 60°$, and similarly, $\theta_i \simeq 40°$ is obtained for the open form.

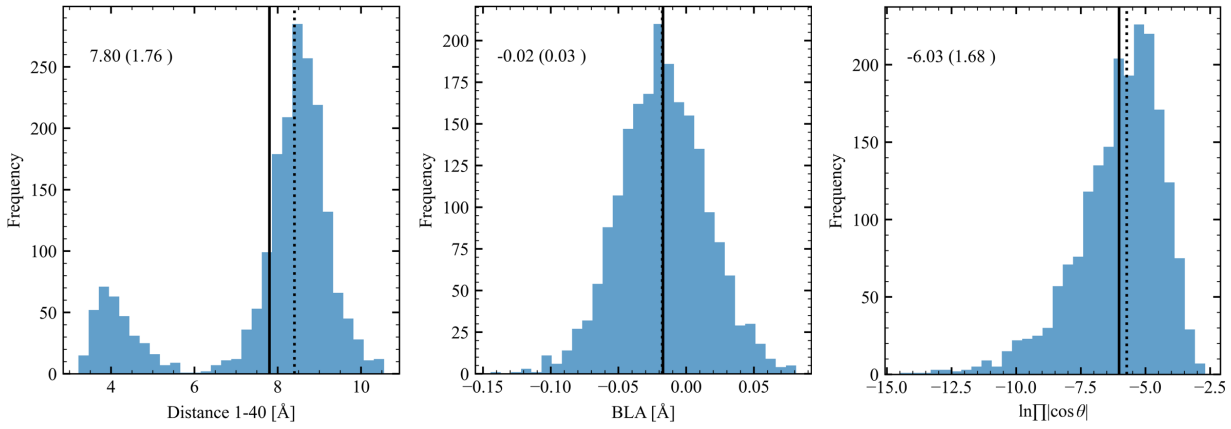

Figure S12: Distributions of structural properties of the **closed** conformer with their respective mean (full line) and median (dashed line). θ_i are the dihedral angles forming the conjugated chain.

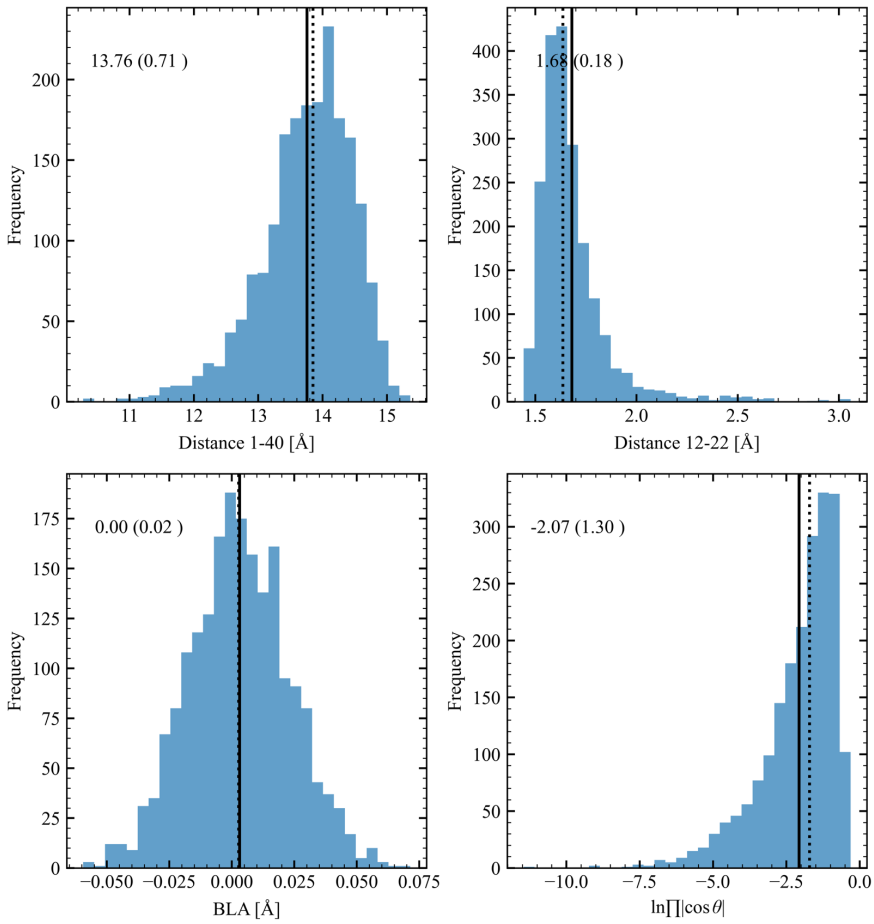

Figure S13: Distributions of structural properties of the **open** conformer with their respective mean (full line) and median (dashed line). θ_i are the dihedral angles forming the conjugated chain.

2.2.3 Structure-NLO properties relationships

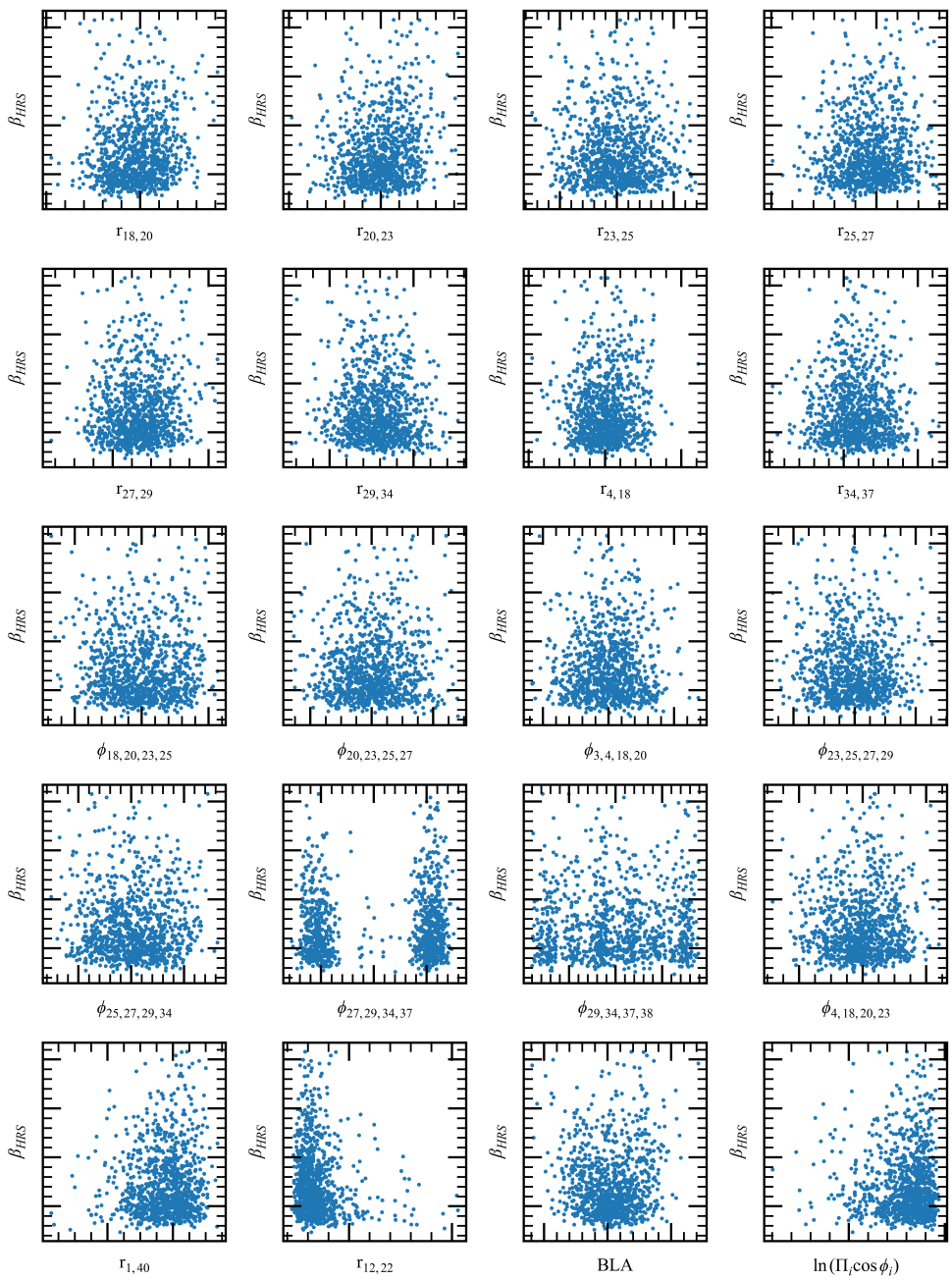

Figure S14: Distribution of β_{HRS} values of the open form as a function of selected structural parameters, as calculated at the MD+DFT[PE] level.

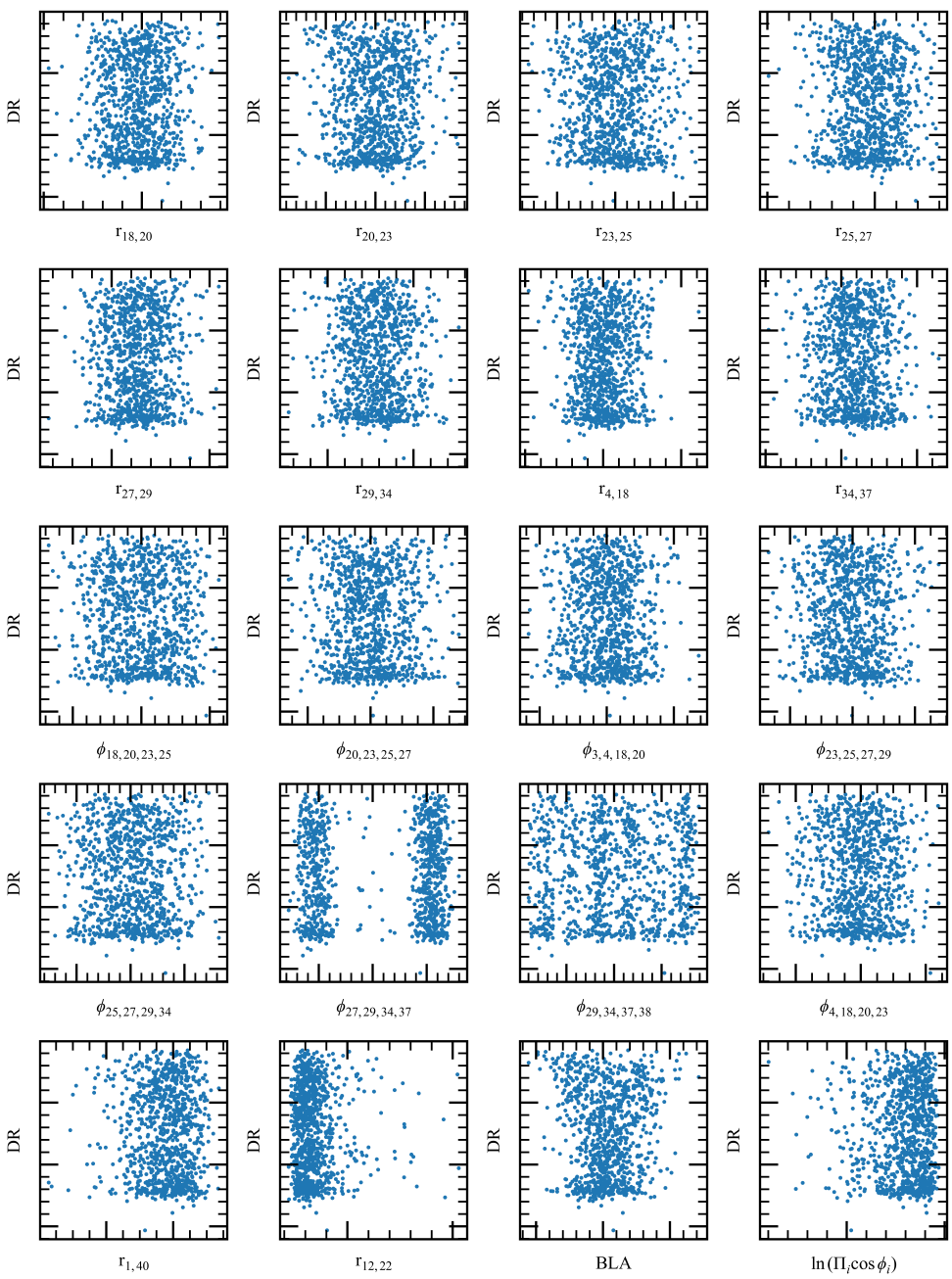

Figure S15: Distribution of DR values of the open form as a function of selected structural parameters, as calculated at the MD+DFT[PE] level.

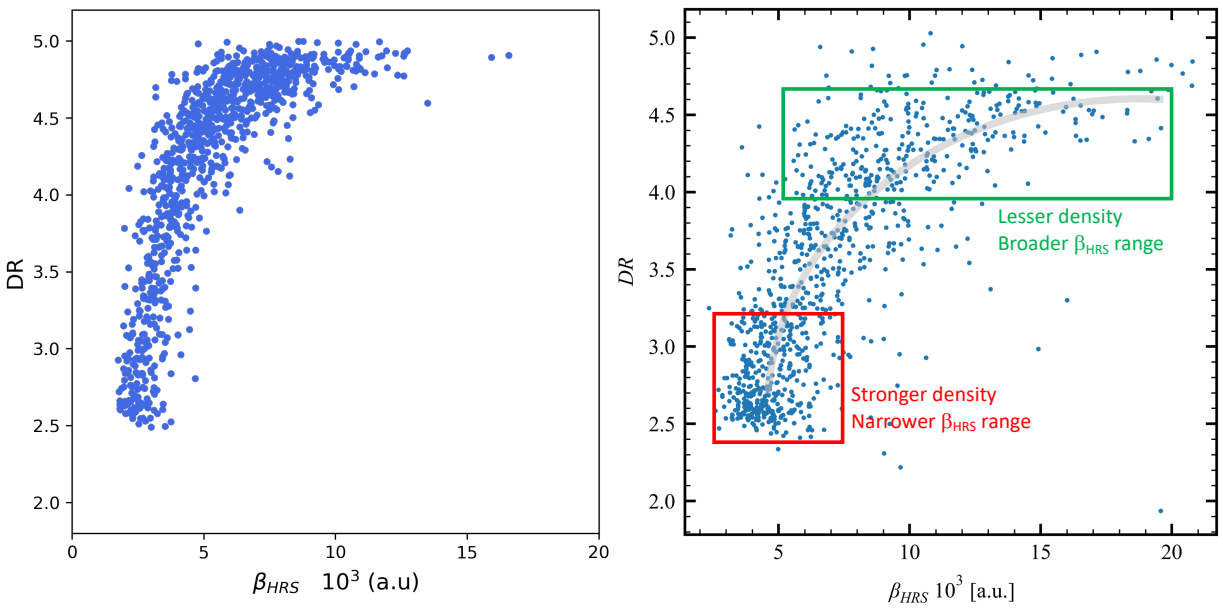

Figure S16: Evolution of β_{HRS} of the open form as a function of DR, as obtained from MD+DFT[gas] (left) and MD+DFT[PE] (right) calculations.

2.3 ONIOM calculations

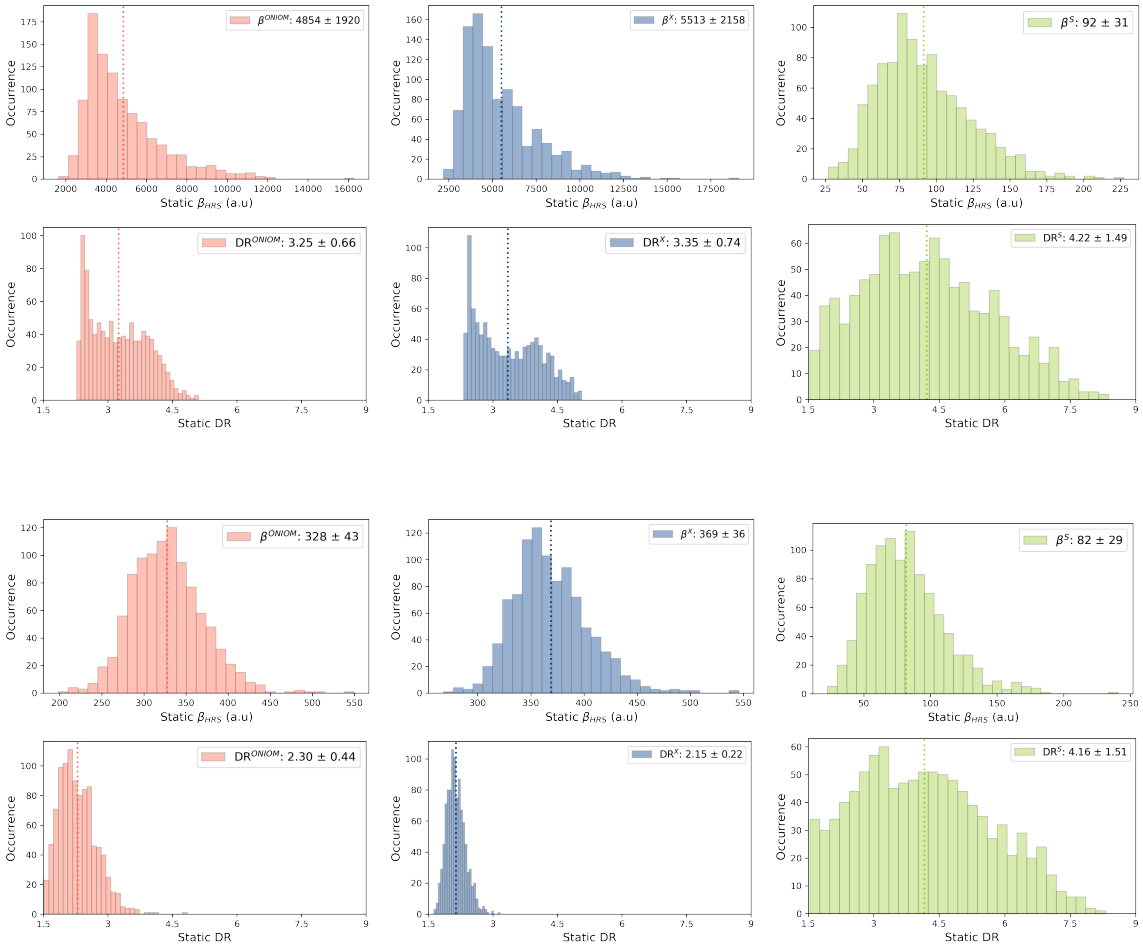

Figure S17: Distributions of the **static** hyperpolarizabilities and depolarization ratios of the total ONIOM (left), chromophore (middle) and solvent (right) contributions calculated for the open (top) and closed (bottom) isomers. Average values are indicated by dotted lines, and standard deviations are given in the legend of each graph. The calculations were performed using the M06-2X XCF.

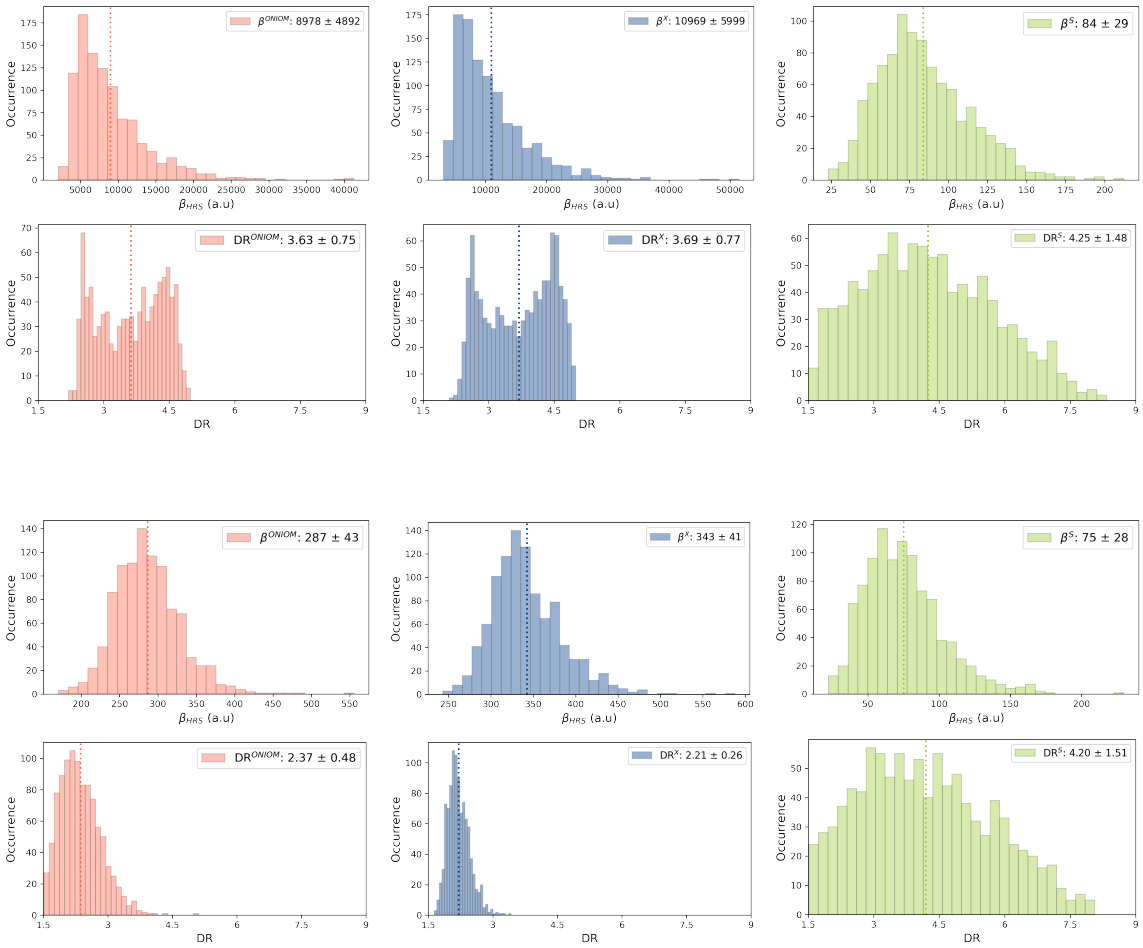

Figure S18: Distributions of the **frequency-dependent** ($\lambda = 1300$ nm) hyperpolarizabilities and depolarization ratios of the total ONIOM (left), chromophore (middle) and solvent (right) contributions calculated for the open (top) and closed (bottom) isomers. Average values are indicated by dotted lines, and standard deviations are given in the legend of each graph. The calculations were performed using the M06-2X XCF.

Table S5: Average values and standard deviations (in a.u.) of the static and frequency-dependent ($\lambda = 1300$ nm) β_{HRS}^{ONIOM}, $\beta_{HRS}^{dressed}$, β_{HRS}^{X} and β_{HRS}^{S} values, calculated for the open and closed isomers. The calculations were performed using the M06-2X XCF.

Open form	$\langle\beta_{HRS}^{ONIOM}\rangle$	$\langle\beta_{HRS}^{dressed}\rangle$	$\langle\beta_{HRS}^{X}\rangle$	$\langle\beta_{HRS}^{S}\rangle$	R^a
dynamic	8978 ± 4892	8977 ± 4892	10969 ± 5999	84 ± 29	0.82
static	4854 ± 1920	4853 ± 1920	5513 ± 2158	92 ± 31	0.88
Closed form	$\langle\beta_{HRS}^{ONIOM}\rangle$	$\langle\beta_{HRS}^{dressed}\rangle$	$\langle\beta_{HRS}^{X}\rangle$	$\langle\beta_{HRS}^{S}\rangle$	R^a
dynamic	287 ± 43	275 ± 46	343 ± 41	75 ± 28	0.80
static	328 ± 43	316 ± 45	369 ± 36	82 ± 29	0.86

[a] $R = \langle\beta_{HRS}^{dressed}\rangle / \langle\beta_{HRS}^{X}\rangle$

Table S6: Average values and standard deviations (in a.u.) of the static and frequency-dependent ($\lambda = 1300$ nm) DR_{HRS}^{ONIOM}, $DR_{HRS}^{dressed}$, DR_{HRS}^{X} and DR_{HRS}^{S} values, calculated for the open and closed isomers. The calculations were performed using the M06-2X XCF.

Open form	$\langle DR_{HRS}^{ONIOM} \rangle$	$\langle DR_{HRS}^{dressed} \rangle$	$\langle DR_{HRS}^{X} \rangle$	$\langle DR_{HRS}^{S} \rangle$	R^a
dynamic	3.63 ± 0.75	3.63 ± 0.75	3.69 ± 0.77	4.25 ± 1.48	0.98
static	3.25 ± 0.66	3.25 ± 0.67	3.35 ± 0.74	4.22 ± 1.49	0.97
Closed form	$\langle DR_{HRS}^{ONIOM} \rangle$	$\langle DR_{HRS}^{dressed} \rangle$	$\langle DR_{HRS}^{X} \rangle$	$\langle DR_{HRS}^{S} \rangle$	R^a
dynamic	2.37 ± 0.48	2.26 ± 0.53	2.21 ± 0.26	4.20 ± 1.51	1.02
static	2.30 ± 0.44	2.21 ± 0.47	2.15 ± 0.22	4.16 ± 1.51	1.03

$^a R = \langle DR_{HRS}^{dressed} \rangle / \langle DR_{HRS}^{X} \rangle$

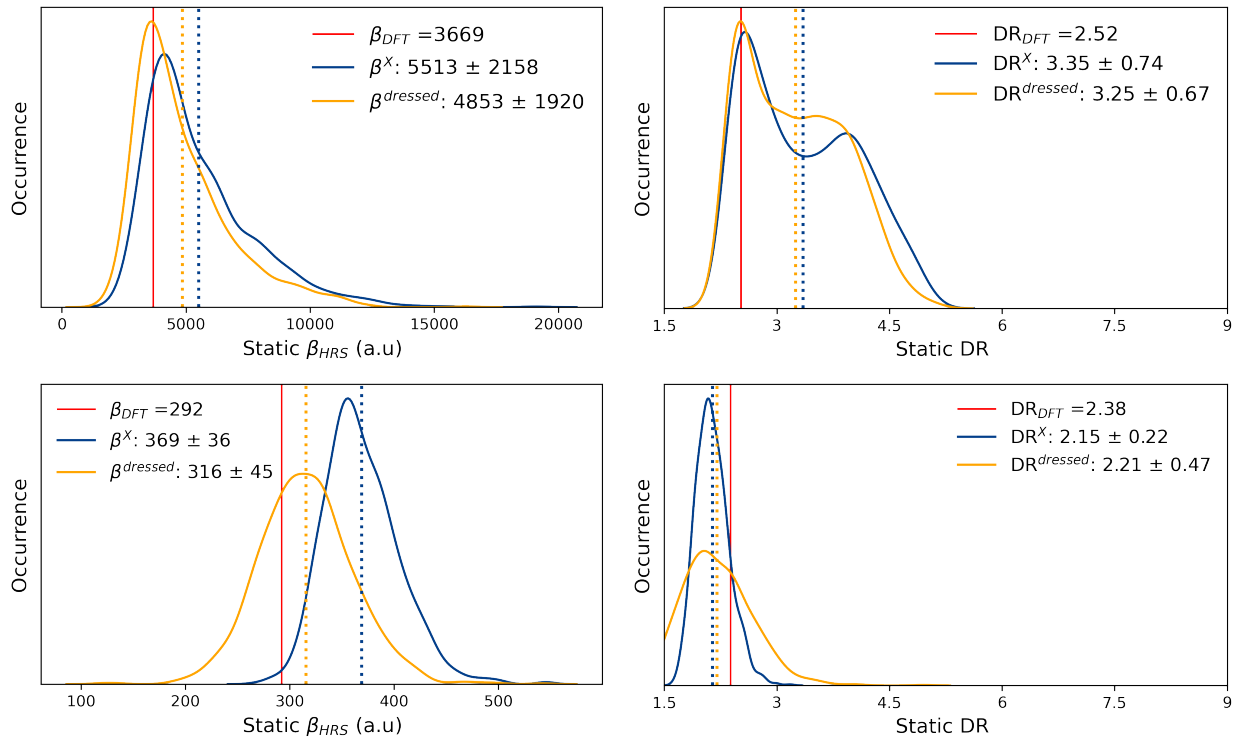

Figure S19: Statistical distributions (kernel density estimations) of the **static** HRS first hyperpolarizability (left) and depolarization ratio (right) of the open (top) and closed (bottom) forms, as calculated using the MD+DFT[SMD] scheme at the M06-2X/6-311+G(d) level for the single chromophore and the dressed quantities as computed using hybrid QM/QM' model. Average values (indicated by dotted lines) and standard deviations are given in the legend of each graph.

References

(S1) Dubuis, S.; Dellai, A.; Courdurié, C.; Owona, J.; Kalafatis, A.; Vellutini, L.; Genin, E.; Rodriguez, V.; Castet, F. Nonlinear Optical Responses of Photoswitchable Donor–Acceptor Stenhouse Adducts. *Journal of the American Chemical Society* **2023**, *145*, 10861–10871.

(S2) Quertinmont, J.; Beaujean, P.; Stiennon, J.; Aidibi, Y.; Leriche, P.; Rodriguez, V.; Sanguinet, L.; Champagne, B. Combining Benzazolo-Oxazolidine Twins toward Multistate Nonlinear Optical Switches. *The Journal of Physical Chemistry B* **2021**, *125*, 3918–3931.

(S3) Bouquiaux, C.; Beaujean, P.; Ramos, T. N.; Castet, F.; Rodriguez, V.; Champagne, B. First hyperpolarizability of the di-8-ANEPPS and DR1 nonlinear optical chromophores in solution. An experimental and multi-scale theoretical chemistry study. *The Journal of Chemical Physics* **2023**, *159*, 174307.

(S4) Castet, F.; Bogdan, E.; Plaquet, A.; Ducasse, L.; Champagne, B.; Rodriguez, V. Reference molecules for nonlinear optics: A joint experimental and theoretical investigation. *Journal of Chemical Physics* **2012**, *136*, 024506.

(S5) Kaatz, P.; Shelton, D. P. Polarized hyper-Rayleigh light scattering measurements of nonlinear optical chromophores. *The Journal of Chemical Physics* **1996**, *105*, 3918–3929.